Robust Longitudinal Power Profile Estimation in Optical Networks using MMSE with Complex Scaling Factor

Inwoong Kim[1], Olga Vassilieva[1], Ryu Shinzaki[2], Motohiko Eto[2], Shoichiro Oda[2], Paparao Palacharla[1]
1. Fujitsu Network Communications, Inc., 2801 Telecom Parkway, Richardson, TX 75082,USA
2. Fujitsu Limited, 1-1 Kamikodanaka 4-Chome, Nakahara-ku, Kawasaki, Kanagawa 211-8588, Japan
inwoong.kim@fujitsu.com

Abstract: We propose a power profile estimator using MMSE, that automatically adjusts the scaling and nonlinear rotation of constellation with complex scaling factor. We demonstrate robust performance in simulation and experiment, even at higher launch powers. © 2023 The Author(s)

1. Introduction

As optical transmission link monitoring becomes important for low margin operation of autonomous and disaggregated optical networks [1-2], there has been active research on longitudinal power profile estimation (PPE) for each wavelength by leveraging coherent optical receiver without the need for any additional hardware such as OTDR [1-6]. PPE based on coherent receiver not only measures power profile in multi-span transmission but also can be used for characterization of gain profile of EDFA/Raman hybrid transmission systems [6]. There are two major approaches of PPE using the coherent receiver [1]. One is based on correlation method (correlation-PPE) and the other one is Minimum Mean Square Error-based method (MMSE-PPE) [1]. In general, two waveforms are compared in both methods, the reference waveform at the receiver side acquired by coherent receiver and the emulated waveform obtained by transmitting optical signal over transmission link in numerical domain. Correlation-PPE finds optimal parameters to estimate power profile by maximizing intensity correlation between the reference waveform and the emulated waveform obtained via single-step digital backpropagation [2]. MMSE-PPE finds optimal parameters via multi-step emulation to estimate power profile by minimizing mean square error between the two waveforms of complex-valued electric field [1, 3-6]. [1] reports that correlation-PPE has limitation in spatial resolution and requires additional calibration process to estimate power profile while MMSE-PPE can directly output absolute longitudinal power profiles with better spatial resolution.

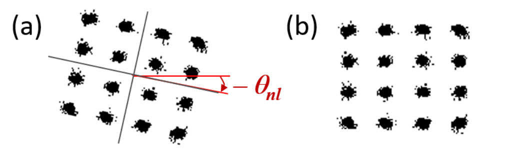

Fig. 1. Constellation at receiver side: (a) with nonlinear rotation θ_{nl} in transmission line, (b) after carrier phase recovery.

Nonlinear transmission over optical fiber causes rotation of the optical signal constellation [7]. In practical applications with coherent receiver, nonlinear rotation, θ_{nl} in Fig. 1(a), of constellation in transmission line cannot be measured because of carrier phase noise (CPN) from finite laser linewidth and environmental perturbation on fiber. Furthermore, carrier phase recovery (CPR) removes CPN and nonlinear rotation θ_{nl} (Fig. 1(b)). This unknown angle θ_{nl} may not be required for correlation-PPE since it evaluates correlation of waveforms in intensity that removes phase information. However, MMSE-PPE requires additional process to estimate the angle θ_{nl} because it compares waveforms of complex-valued electrical fields [6]. We propose an elegant solution for this problem by introducing complex scaling factor that can automatically adjust scaling and nonlinear rotation of constellation for robust operation of PPE. We demonstrate its improved and robust performance in simulation and experiment, including reliable anomaly loss detection in transmission links.

2. Impact of Unknown Nonlinear Rotation of Constellation in MMSE-PPE

The unknown nonlinear rotation, θ_{nl}, can cause problem in MMSE-PPE that finds optimal parameters minimizing errors between the emulated and the received reference waveforms because nonlinear interference noise and nonlinear rotation of constellation occur in transmission [7], that depends on dispersion and power profile.

To illustrate the impact of nonlinear rotation of constellation in MMSE-PPE, a 96 Gbaud DP-16QAM is transmitted over 5 spans of 80 km SMF links with ideal noiseless optical amplifiers. Dispersion of fiber is about 17 ps/nm/km, nonlinear coefficient is 1.3 /W/km, fiber attenuation is 0.2 dB/km. Launch power is set as 0 dBm or 4.8 dBm. Split-step Fourier method is used for transmission simulation with 8 samples per symbol and step size of 0.1 km. Conventional MMSE-PPE (C-MMSE-PPE) based on [3] is used with 60 steps per span and 2 samples per symbol. The estimated results are smoothed by taking moving average over 5 points. The number of symbols is 2^{13}. Figure 2 (a) shows the estimated power profile (C-MMSE-PPE with circular and cross markers), when the nonlinear rotation, θ_{nl}, is ignored at the received waveform. The PPE shows clear discrepancy with theoretical expectation (red dashed line) based on fiber span and attenuation. C-MMSE-PPE, black solid and green dashed lines in Fig. 2 (a), shows the estimated power profile when the nonlinear rotation found in simulation is considered. The PPE shows good agreement with theory; however, it starts to show a bit noisy result at 4.8 dBm (black line) possibly due to stability of solution and may require larger number of symbols for better accuracy.

As shown in these examples, estimation of nonlinear rotation, θ_{nl}, is required for proper operation of C-MMSE-PPE.

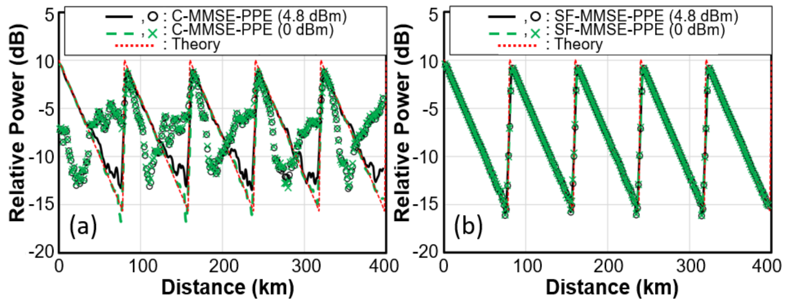

Fig. 2. Estimated power profiles (black solid and green dashed lines: with known θ_{nl}, circular and cross markers: without known θ_{nl}): (a) C-MMSE-PPE, (b) SF-MMSE-PPE.

3. MMSE-PPE with Complex Scaling Factor

Linear least square method is used in [3] to solve MMSE for PPE. We modify the linear least square method by introducing a complex scaling factor that can properly model the emulated waveform by taking into consideration the nonlinear rotation, θ_{nl}, and normalization errors of constellation in PPE. We explained the difficulty of measuring θ_{nl} in introduction. Normalization error may not be expected normally, but it can happen in certain circumstances. As an example, if transmitter characteristics such as frequency response with limited bandwidth is not fully characterized, then reconstructed waveform at transmitter based on received symbols may have some errors which can cause normalization error.

Let us assume $A(z_k, m)$ is optical signal where z_k is location and m is the sampling sequence. $A(z_0 = 0, m)$ and $A(z_N = L, m)$ are complex-valued waveforms at transmitter and receiver respectively, where there are M samples in each waveform and N segments along the transmission line. The solution describing emulation of propagation based on nonlinear Schrödinger can be found as

$$A(L,m) \approx \widehat{H}(L)A(0,m) - \sum_{k=0}^{N-1} j\gamma'_k \Delta z_k \left\{\widehat{H}(L-z_k)\left[\widehat{N}\left(\widehat{H}(z_k)A(0,m)\right)\right]\right\} \quad (1)$$

considering first order perturbation terms only as described in [3], where $\widehat{H}(z)$ is a linear operator describing chromatic dispersion for the propagation of distance z and $\widehat{N}$ is nonlinear operator $\|\cdot\|^2$, Δz_k is the step size of segment, and $\gamma'_k = -\gamma_{nl}\exp[\int_0^{z_k}\alpha(z)dz]$. $\alpha(z)$ is attenuation in fiber and γ_{nl} is nonlinear coefficient of fiber such that γ'_k is proportional to optical power at z_k when power of $A(z_k, m)$ is normalized. Now, let us introduce a *complex scaling factor* $\rho e^{j\theta}$ in Eq. (1), then

$$A(L,m) \approx \rho e^{j\theta}\widehat{H}(L)A(0,m) - \rho e^{j\theta}\sum_{k=0}^{N-1} j\gamma'_k \Delta z_k \left\{\widehat{H}(L-z_k)\left[\widehat{N}\left(\widehat{H}(z_k)A(0,m)\right)\right]\right\} \quad (2)$$

To rewrite Eq. (2) in simpler form, let us define $g[z_k, m] = -j\Delta z_k \left\{\widehat{H}(L-z_k)\left[\widehat{N}\left(\widehat{H}(z_k)A(0,m)\right)\right]\right\}$, where $m = 0, \ldots, M$ and $k = 0, 1, \ldots, N-1$. We define $(\boldsymbol{G})_{mk} = g[z_k, m]$ for $k < N$ and $(\boldsymbol{G})_{mN} = \widehat{H}(L)A(0,m)$, $\boldsymbol{\gamma}" = \rho e^{j\theta}[\gamma'_0, \gamma'_1, \ldots, \gamma'_{N-1}, 1]^T$ where $\gamma"_N = \rho e^{j\theta}$, and $\boldsymbol{A} = [A(L,0), A(L,1), \ldots, A(L,M)]^T$. Then the Eq. (2) becomes

$$\boldsymbol{A} \approx \boldsymbol{G}\boldsymbol{\gamma}" \quad (3)$$

In estimation of $\boldsymbol{\gamma}"$, we minimize $I \approx E[\|\boldsymbol{A} - \boldsymbol{G}\boldsymbol{\gamma}"\|^2]$ or difference between two sides in Eq. (3) where left side is reference waveform at receiver side and the right side is emulated one by propagation of transmitter-side waveform. The solution of Eq. (3) minimizing I is well known as

$$\widehat{\boldsymbol{\gamma}"} = [\boldsymbol{G}^\dagger\boldsymbol{G}]^{-1}\boldsymbol{G}^\dagger\boldsymbol{A} \quad (4)$$

Finally, power profile is proportional to absolute value of $[\gamma"_0, \gamma"_1, \ldots, \gamma"_{N-1}]/\gamma"_N$ where $\gamma"_N$ is optimal complex scaling factor taking care of scaling and nonlinear rotation of constellation. This proposed method with scaling factor is denoted as SF-MMSE-PPE in the rest of the paper.

4. Evaluation of Proposed SF-MMSE-PPE

4.1. Simulation Results

The proposed SF-MMSE-PPE is applied to the simulation example in section 2. The results, in Fig. 2 (b) with legend SF-MMSE-PPE, show consistent estimation of PPE as expected without regard to unknown nonlinear rotation of constellation. In addition, we found that estimated power profile is better for higher launch power of 4.8 dBm. We tried even higher launch power of 15 dBm and found that SF-MMSE-PPE still worked while C-MMSE-PPE failed (not shown due to limited space). The reason why SF-MMSE-PPE shows better result at higher launch power is due to the larger solution space considered in (4). The SF-MMSE-PPE method does not limit to real valued solution only as in C-MMSE-PPE. These simulation results show the clear benefit of modeling with complex scaling factor in SF-MMSE-PPE.

4.2. Experimental Results

Experimental setup is shown in Fig. 3. Channel under test (CUT), with 96 Gbaud DP-16QAM, is transmitted over 5 spans of 80 km SMF with 44 neighboring channels at 100 GHz spacing loaded with shaped ASE noise by WSS filter. An additional variable attenuator is added in the middle of third span to emulate anomaly loss. Launch power is set as 2.8 dBm or 4.8 dBm per channel. The received OSNR is 30 dB. Arbitrary waveform generator is used for CUT to generate data with Nyquist pulse shaping at transmitter. Digital storage scope is used to sample data from coherent detection. Stored data is processed off-line. Training symbols and pilot symbols are added for adaptive equalizer and CPR. One sample per symbol, just like shown in Fig. 1 (b), is used for SF-MMSE-PPE assuming hardware limitations in data transfer for analytics. The reference waveform at the receiver is obtained by applying chromatic dispersion of transmission link after upsampling with zero padding in frequency domain. Simple hard decision is used to determine transmitted symbols, then the waveform at the transmitter is reconstructed by applying Nyquist pulse shaping. But frequency response of all the components in transmitter is not characterized, thus just flat frequency response is assumed. A total number of 40 waveforms with 722400 symbols are processed and averaged over the number of waveforms to find the longitudinal power profile.

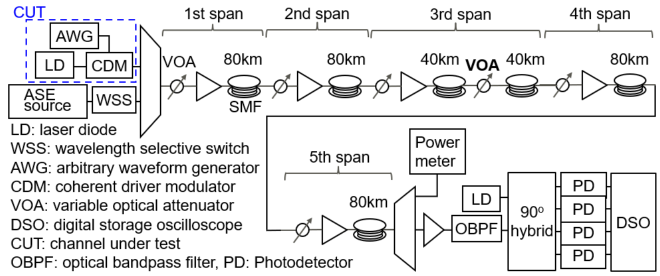

Fig. 3. Schematic diagram of experimental setup.

Figure 4 (a) shows good agreement between the results (black solid and green dashed lines) by SF-MMSE-PPE and theoretical profile (red dashed line) except some regions where nonlinear interference is small due to lower optical power, while C-MMSE-PPE shows big discrepancy (yellow line). We also found that there was about 10% error in normalization of waveforms due to unknown factors in transmitter. In the region where optical power is small due to attenuation, SF-MMSE-PPE with 4.8 dBm launch power shows better result (as highlighted with blue circle in Fig. 4 (a)) than with smaller launch power because of difference in nonlinear interference. Experimental results also confirm reliable operation of SF-MMSE-PPE without the need to know the nonlinear rotation, θ_{nl}, thereby simplifying the implementation. Figure 4 (b) shows the estimated power profile by SF-MMSE-PPE depending on anomaly loss at the third span (no loss or 3 dB loss at 40 km), which confirms reliable detection of anomaly loss by closely overlapped profiles except the region affected by anomaly loss (green circle).

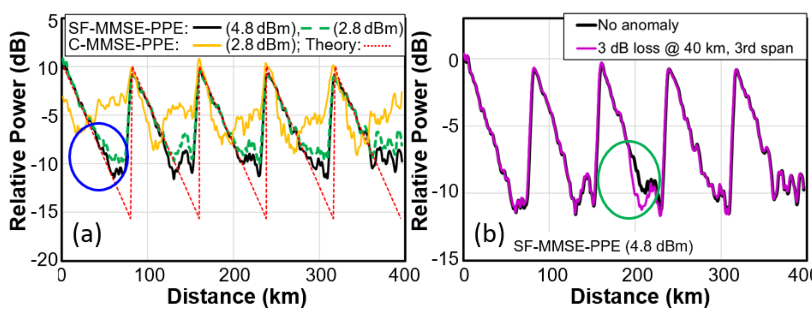

Fig. 4. Estimated power profiles using SF-MMSE-PPE: (a) depending on launch power, (b) depending on anomaly loss.

5. Conclusion

We proposed a robust MMSE-PPE by introducing a complex scaling factor that automatically adjusts scaling and nonlinear phase rotation, θ_{nl}, of constellation for waveforms. In practical coherent systems, we cannot measure θ_{nl} of constellation that affects accuracy of conventional MMSE-PPE. The SF-MMSE-PPE showed robust estimation of longitudinal power profiles in simulation and experiment, even at higher launch powers. It is envisioned that reliable anomaly detection and localization from this PPE technique can simplify operations of disaggregated optical networks.

6. References

[1] T. Sasai, "Digital Longitudinal Monitoring of Optical Transmission Link," in Proc. of ECOC 2022, Th1D.1, (2022).
[2] T. Tanimura *et al.*, "Experimental Demonstration of a Coherent Receiver that Visualizes Longitudinal Signal Power Profile over Multiple Spans out of Its Incoming Signal," in Proc. of ECOC 2019, PD3.4, (2019).
[3] T. Sasai *et al.*, "Proposal of Linear Least Squares for Fiber-Nonlinearity-Based Longitudinal Power Monitoring in Multi-Span Link," in Proc. of OECC 2022, WB3-1, (2022).
[4] S. Gleb *et al.*, "Fiber link anomaly detection and estimation based on signal nonlinearity," in Proc. of ECOC 2021, Tu2C2.5, (2021).
[5] M. Eto *et al.*, "Location-resolved PDL Monitoring with Rx-side Digital Signal Processing in Multi-span Optical Transmission System," in Proc. of OFC 2022, Th1C.2, (2022).
[6] T. Sasai *et al.*, "Digital Longitudinal Monitoring of Optical Fiber Communication Link," *J. Light. Tech.*, vol. 40, no. 8, pp. 2390-2408, 2022.
[7] P. Minzioni *et al.*, "Study of the Gordon–Mollenauer Effect and of the Optical-Phase-Conjugation Compensation Method in Phase-Modulated Optical Communication Systems", *IEEE Photon. J.*, vol. 2, no. 3, pp. 284-291, 2010.